30 hours after infection of mosquitoes lacking LRIM1, APL1, or TEP1. As reported previously (*16*), three distinct classes of parasites were observed in the midguts of control mosquitoes: live (GFP positive), dead (TEP1 positive), and dying (GFP and TEP1 positive). In contrast, TEP1-positive parasites were never detected in *LRIM1* or *APL1* KD mosquitoes (Fig. 3C), despite the presence of TEP1-F in the hemolymph. Lack of TEP1 parasite staining was as complete as in TEP1 KD mosquitoes, which entirely lack TEP1 in the hemolymph. These data demonstrate that the LRIM1/APL1C complex is necessary for TEP1-mediated parasite killing during midgut invasion and indicate that TEP1 binds parasites only after it is processed.

The *APL1* locus has been implicated in mosquito resistance to the human malaria parasite, *Plasmodium falciparum* (*6*), and TEP1 has been shown to act against *P. falciparum* in laboratory infections (*7*). Mosquito defense against *Plasmodium* is likely to be influenced by vector/parasite coevolution and adaptation; thus, the observation that LRIM1 did not affect *P. falciparum* in experimental field infections (*17*) may suggest that parasites have evolved to evade this pathway. Proteins such as the fibrinogen-related FBN9 (*18*) or other LRR proteins may provide alternative mechanisms for TEP1-mediated parasite killing.

Bioinformatic searches for proteins related to LRIM1 and APL1C using their shared structural features (signal peptide, LRRs, cysteine pattern, and coiled-coils) (see supporting online material) detected more than 20 *LRIM*-like genes in each of the available mosquito genomes—*A. gambiae*, *Aedes aegypti*, and *Culex quinquefasciatus*—but not in any other species (table S1). Several of these genes were previously implicated in *A. gambiae* immune responses (*3*, *6*, *7*, *9*, *19*). Phylogenetic analysis in conjunction with pairwise comparisons, examination of orthologous genomic neighborhoods, and protein domain analysis revealed four distinct LRIM subfamilies (figs. S3 and S4). Thus, LRIM1 and APL1C are members of a family of putative recognition receptors, which appears to be unique and greatly expanded in mosquitoes. Nevertheless, structural integrity of both LRRs and coiled-coils rests with only a few key amino acids, allowing considerable sequence variation that may hinder identification of functional equivalents in other organisms.

The versatile LRR motif mediates recognition of diverse pathogen-associated molecules in host innate defense in plants and animals (*20*). For example, the repertoire of variable lymphocyte receptor (VLR) antibodies in jawless vertebrates is generated by combinatorial assembly of LRR modules instead of immunoglobulin segments as in jawed vertebrates (*21*). Similarly to LRIM1/APL1C, the VLR antibodies are secreted as disulfide-linked multimers (*22*).

LRIMs form a family of mosquito LRR receptors with putative roles in defense against human and animal pathogens. LRIM1 and APL1C exist as a complex that mediates immunity against malaria parasites through activation of mosquito complement. The multimeric nature of the complex indicates the potential to bind multiple targets similarly to mammalian multisubunit receptors that robustly activate complement, that is, immunoglobulin M, lectin, and C1q. Bound LRIM1/APL1C complex may then undergo conformational changes inducing the recruitment of additional cascade components, such as a TEP1-activating protease. In-depth study of these interactions will provide insights into complement activation in mosquitoes and tools toward blocking disease transmission.

References and Notes

1. R. W. Snow, C. A. Guerra, A. M. Noor, H. Y. Myint, S. I. Hay, *Nature* **434**, 214 (2005).
2. S. A. Blandin, E. Marois, E. A. Levashina, *Cell Host Microbe* **3**, 364 (2008).
3. M. A. Osta, G. K. Christophides, F. C. Kafatos, *Science* **303**, 2030 (2004).
4. E. Warr, L. Lambrechts, J. C. Koella, C. Bourgouin, G. Dimopoulos, *Insect Biochem. Mol. Biol.* **36**, 769 (2006).
5. L. F. Moita *et al.*, *Immunity* **23**, 65 (2005).
6. M. M. Riehle *et al.*, *Science* **312**, 577 (2006).
7. Y. Dong *et al.*, *PLoS Pathog.* **2**, e52 (2006).
8. T. Habtewold, M. Povelones, A. M. Blagborough, G. K. Christophides, *PLoS Pathog.* **4**, e1000070 (2008).
9. M. M. Riehle *et al.*, *PLoS One* **3**, e3672 (2008).
10. F. H. Collins *et al.*, *Science* **234**, 607 (1986).
11. G. Dimopoulos, A. Richman, H. M. Muller, F. C. Kafatos, *Proc. Natl. Acad. Sci. U.S.A.* **94**, 11508 (1997).
12. H. M. Muller, G. Dimopoulos, C. Blass, F. C. Kafatos, *J. Biol. Chem.* **274**, 11727 (1999).
13. S. Blandin *et al.*, *Cell* **116**, 661 (2004).
14. E. A. Levashina *et al.*, *Cell* **104**, 709 (2001).
15. R. H. Baxter *et al.*, *Proc. Natl. Acad. Sci. U.S.A.* **104**, 11615 (2007).
16. C. Frolet, M. Thoma, S. Blandin, J. A. Hoffmann, E. A. Levashina, *Immunity* **25**, 677 (2006).
17. A. Cohuet *et al.*, *EMBO Rep.* **7**, 1285 (2006).
18. Y. Dong, G. Dimopoulos, *J. Biol. Chem.* www.jbc.org/cgi/doi/10.1074/jbc.M807084200. Published online 4 February 2009.
19. R. Aguilar *et al.*, *Insect Biochem. Mol. Biol.* **35**, 709 (2005).
20. T. Nurnberger, F. Brunner, B. Kemmerling, L. Piater, *Immunol. Rev.* **198**, 249 (2004).
21. Z. Pancer *et al.*, *Nature* **430**, 174 (2004).
22. B. R. Herrin *et al.*, *Proc. Natl. Acad. Sci. U.S.A.* **105**, 2040 (2008).

23. The authors thank A. C. Koutsos for generating the LRIM1 antibody and sharing it before publication and F. M. Ausubel for critically reviewing the manuscript. Fluorescence microscopy was performed at the Imperial College Facility for Imaging by Light Microscopy imaging facility. This work was supported by a Wellcome Trust Program grant (GR077229/Z/05/Z), an NIH Program Project (2PO1AI044220-06A1), and a Biotechnology and Biological Sciences Research Council grant (BB/E002641/1). R.M.W. was supported by a Wellcome Trust Ph.D. fellowship.

Supporting Online Material

www.sciencemag.org/cgi/content/full/1171400/DC1
Materials and Methods
Figs. S1 to S4
Table S1
References

26 January 2009; accepted 24 February 2009
Published online 5 March 2009;
10.1126/science.1171400
Include this information when citing this paper.

Glioma-Derived Mutations in *IDH1* Dominantly Inhibit IDH1 Catalytic Activity and Induce HIF-1α

Shimin Zhao,[1,2] Yan Lin,[1]* Wei Xu,[1,2]* Wenqing Jiang,[1,2]* Zhengyu Zha,[1] Pu Wang,[1,2] Wei Yu,[1,2] Zhiqiang Li,[4] Lingling Gong,[5] Yingjie Peng,[6] Jianping Ding,[6] Qunying Lei,[1,3] Kun-Liang Guan,[1,3,7]† Yue Xiong[1,2,8]†

Heterozygous mutations in the gene encoding isocitrate dehydrogenase-1 (*IDH1*) occur in certain human brain tumors, but their mechanistic role in tumor development is unknown. We have shown that tumor-derived *IDH1* mutations impair the enzyme's affinity for its substrate and dominantly inhibit wild-type IDH1 activity through the formation of catalytically inactive heterodimers. Forced expression of mutant *IDH1* in cultured cells reduces formation of the enzyme product, α-ketoglutarate (α-KG), and increases the levels of hypoxia-inducible factor subunit HIF-1α, a transcription factor that facilitates tumor growth when oxygen is low and whose stability is regulated by α-KG. The rise in HIF-1α levels was reversible by an α-KG derivative. HIF-1α levels were higher in human gliomas harboring an *IDH1* mutation than in tumors without a mutation. Thus, IDH1 appears to function as a tumor suppressor that, when mutationally inactivated, contributes to tumorigenesis in part through induction of the HIF-1 pathway.

Gliomas are the most common type of human brain tumors and can be classified based on clinical and pathological criteria into four grades. The grade IV glioma, commonly known as glioblastoma multiforme (GBM), has one of the worst prognoses among all types of human tumors and can develop either de novo (primary GBM) or through progression from low-grade tumors (secondary GBM). Although pathologically indistinguishable, primary and secondary GBM exhibit distinct patterns of cancer gene alterations (*1*). A recent cancer genome sequencing project revealed that the gene encoding *IDH1* is somatically mutated predominantly in secondary GBM (*2*). Three subsequent studies of targeted *IDH1* gene sequencing confirmed this finding, together identifying *IDH1* mutations in more than 70% of secondary GBM or low-grade gliomas but

infrequently in primary GBM (about 5%) (*3*–*5*). Notably, all of the *IDH1* mutations identified to date produce a single amino acid substitution at Arg^{132} (R132) and no obvious inactivating (frameshift or protein-truncation) mutations were found. This observation, together with the fact that the tumors do not show loss-of-heterozygosity (LOH), has led to speculation that R132 mutations lead to oncogenic activation of the enzyme.

IDH enzymes catalyze the oxidative decarboxylation of isocitrate (ICT) to produce α-KG. The human genome has five *IDH* genes coding for three distinct IDH enzymes whose activities are dependent on either nicotinamide adenine dinucleotide phosphate ($NADP^+$-dependent IDH1 and IDH2) or nicotinamide adenine dinucleotide (NAD^+-dependent IDH3). Both IDH2 and IDH3 enzymes are localized in the mitochondria and participate in the citric acid (TCA) cycle for energy production, whereas IDH1 is localized in the cytoplasm and peroxisomes (*6*). The R132 residue is conserved in all $NADP^+$-dependent IDHs.

To explore the functional impact of the tumor-associated mutations at R132, we performed modeling studies based on the previously reported human cytosolic IDH1 crystal structure (*7*). Among all residues involved in binding with ICT, the side chain of R132 uniquely forms three hydrogen bonds with both the α- and β-carboxyl groups of the substrate ICT, whereas other residues involved in ICT binding form no more than two hydrogen bonds (Fig. 1A). Substitution of R132 with any one of the six amino acids observed in gliomas (His, Ser, Gly, Cys, Val, and Leu) would impair interactions of the enzyme with ICT both sterically and electrostatically. Representative modeling of H132, which corresponds to the most prevalent *IDH1* mutation in human gliomas, is shown in Fig. 1A. We determined the in vitro enzymatic activities of three tumor-derived IDH1 mutants, R132H, R132C and R132S, expressed in transformed human embryonic kidney (HEK) 293T cells and found that all three mutants have a greater than 80% reduction in activity as compared with the wild-type (WT) IDH1 (Fig. 1B). Analysis of recombinant IDH1 mutant proteins purified from *Escherichia coli* likewise displayed little activity in vitro compared with wild-type controls (Fig. 1B). Kinetic analyses of recombinant IDH1 proteins revealed that all three mutant IDH1s had a dramatically reduced affinity for ICT: The Michaelis constants (K_ms) of $IDH1^{R132C}$, $IDH1^{R132S}$, and $IDH1^{R132H}$ for ICT were increased by factors of 60, 70, and 94, respectively (Fig. 1C). In contrast, the K_m for $NADP^+$ and the maximum velocity (V_{max}) were not appreciably altered (Fig. 1C). Similarly, mutation of an arginine residue in pig mitochondrial IDH2 equivalent to R132 in human IDH1 caused a dramatic increase in K_m for isocitrate (by a factor of 165), with minimal effect on V_{max} (*8*). Because the normal cellular concentration of ICT is 20 to 30 μM (*9*), which is lower than the K_m of the IDH1 mutants, the mutant enzymes are likely to have limited activity under physiological conditions. Together, these structural and biochemical analyses indicate that the tumor-associated *IDH1* mutations inactivate the enzyme.

Given that IDH1 normally functions as a homodimer, we hypothesized that the mutant IDH1 molecules in tumor cells form heterodimers with wild-type molecules and, in so doing, dominantly inhibit the activity of wild-type IDH1. To test this hypothesis, we coexpressed His-tagged wild-type and FLAG-tagged R132H mutant *IDH1* in *E. coli* and isolated the heterodimer by sequential affinity purification using first nickel resin and then FLAG beads. Formation of either WT:WT homodimer or WT:R132H heterodimer was confirmed by gel filtration (fig. S1). As expected, the WT:WT homodimers were fully active and the R132H:R132H homodimers were nearly completely inactive (Fig. 2A). Notably, the WT:R132H heterodimer exhibited only 4% of the activity shown by the wild-type enzyme when assayed with limited ICT concentration (Fig. 2A). Normally, IDH1 can adopt at least three distinct conformations during catalysis: a quasi-open conformation when it is in a complex with $NADP^+$, a quasi-closed conformation when it is in a complex with ICT, and a closed conformation when it is in a complex with both $NADP^+$ and ICT (fig. S2A) (*7*). The two IDH1 subunits act in a cooperative manner and undergo conformational changes in a concerted way. Our modeling study suggests that the impairment in enzyme binding with ICT conferred by the R132 mutation in one subunit might also impair the binding of ICT to the second wild-type subunit. As a result, both subunits would be locked in an unliganded or quasi-open ($NADP^+$-bound) conformation, thereby inhibiting catalytic activity (Fig. 2B for the close-up of the catalytic active site) (fig. S2, B and C). Consistent with this model, we found that the wild-type IDH1 exhibits a sigmoidal curve of cooperative binding to ICT, whereas the WT:R132H heterodimer displayed a hy-

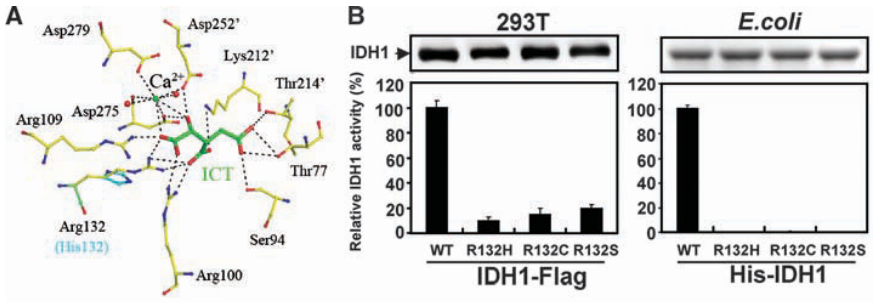

C

IDH1	WT	R132H	R132S	R132C
Km isocitrate (μM)	6.2 ± 1	582.4 ± 56.1	434.1 ± 12.2	368.6 ± 20.6
Km $NADP^+$ (μM)	7.3 ± 0.6	12.2 ± 3.8	14.4 ± 2.2	6.8 ± 2.0
Vmax μmol.min^{-1}.mg^{-1}	56.9 ± 6.6	31.9 ± 3.2	48.0 ± 1.8	57.5 ± 5.7

Fig. 1. Tumor-derived IDH1 mutants have reduced catalytic activity because of impaired isocitrate binding. (**A**) Structural modeling predicts that mutation of R132 in IDH1 would weaken hydrogen bonding of the enzyme to ICT. Shown is a view of the catalytic active site of human IDH1 bound with $NADP^+$ (omitted for clarity), ICT (green), and Ca^{2+}. The residues interacting with ICT from the adjacent subunit are labeled with an apostrophe. Hydrogen-bonding interactions are indicated with dashed lines. Simulated H132 mutation (cyan) is superimposed on R132. (**B**) Tumor-derived IDH1 mutants have reduced catalytic activity in vitro. Left, FLAG-tagged wild-type and mutant IDH1 were expressed in HEK293T cells, purified by immunoprecipitation and eluted by FLAG peptide; right, HIS-tagged wild-type and mutant IDH1 were expressed in *E. coli* and purified by nickel resin. Specific IDH1 activities for all proteins were measured in the presence of $NADP^+$ (10 μM) and ICT (30 μM), with the presence of 2 mM Mn^{2+}. Shown are mean values of triplicate experiments ±SD. (**C**) Kinetic parameters of wild-type and mutant IDH1. Shown are mean values of duplicate experiments ±SD.

[1]Molecular and Cell Biology Laboratory, Institute of Biomedical Sciences, Fudan University, 130 Dong-An Road, Shanghai 200032, China. [2]School of Life Sciences, Fudan University, 220 Han-Dan Road, Shanghai 200433, China. [3]Department of Biological Chemistry, School of Medicine, Fudan University, 130 Dong-An Road, Shanghai 200032, China. [4]Department of Neurosurgery, Zhongnan Hospital, Wuhan University, Wuhan 430071, China. [5]Department of Pathology, Zhongnan Hospital, Wuhan University, Wuhan 430071, China. [6]State Key Laboratory of Molecular Biology, Institute of Biochemistry and Cell Biology, Shanghai Institute for Biological Sciences, Chinese Academy of Sciences, 320 Yue-Yang Road, Shanghai 200031, China. [7]Department of Pharmacology and Moores Cancer Center, University of California San Diego, La Jolla, CA 92093, USA. [8]Department of Biochemistry and Biophysics, Lineberger Comprehensive Cancer Center, University of North Carolina at Chapel Hill, NC 27599, USA.

*These authors contributed equally to this work.

†To whom correspondence should be addressed. E-mail: kuguan@ucsd.edu (K.-L.G.); yxiong@email.unc.edu (Y.X.)

perbolic curve with a much higher K_m (Fig. 2C), indicating that the heterodimer not only loses affinity but also cooperativity toward ICT.

We next investigated whether loss of IDH1 activity would alter cellular levels of α-KG, the product of IDH1 catalysis. We used RNA interference to down-regulate endogenous *IDH1* and determined the α-KG levels in U-87MG human glioblastoma cells. Two independent short hairpin RNAs (shRNAs) decreased *IDH1* mRNA by more than 75% and reduced cellular α-KG levels by up to 50% (fig. S3). Expression of the IDH1^{R132H} mutant at a level similar to the endogenous protein (fig. S4A) in the cytoplasm of U-87MG cells caused a dose-dependent reduction of α-KG levels (Fig. 2D) (fig. S4, A and B). Together, these data indicate that tumor-derived mutant IDH1 dominantly inhibits the wild-type IDH1 by forming a catalytically inactive heterodimer, resulting in a decrease of cellular α-KG.

Because α-KG is required by prolylhydroxylases (PHD), enzymes that hydroxylate and promote the degradation of hypoxia-inducible

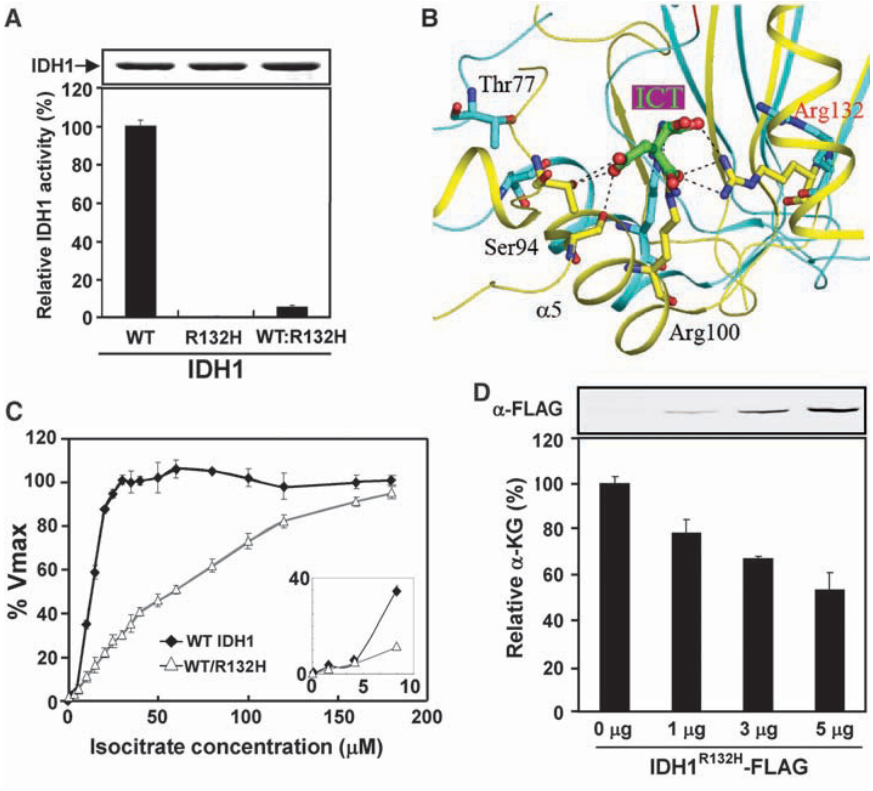

Fig. 2. The R132H mutation dominantly inhibits IDH1 activity and reduces cellular levels of α-KG. (**A**) The WT:R132H heterodimer of IDH1 has low specific activity. The specific activities of WT:WT, R132H:R132H, and WT:R132H dimers were measured under conditions of $NADP^+$ (10 μM), ICT (30 μM), and 2 mM $MnCl_2$. Activities were normalized by protein levels, and wild-type activity was arbitrarily set as 100%. Shown are mean values of triplicate experiments ±SD. (**B**) A close-up view showing the conformational differences between the IDH1-$NADP^+$ and IDH1-$NADP^+$-ICT complexes at the active site. The enzyme adopts a quasi-open conformation in the IDH1-$NADP^+$ complex (cyan) and a closed conformation in the IDH1-$NADP^+$-ICT complex (yellow). The bound ICT and the side chains of several residues in IDH1 involved in ICT binding are shown. (**C**) The WT:R132H heterodimer loses cooperative binding to ICT. The activities of the WT:WT and WT:R132H enzymes were assayed with increasing concentrations of ICT in the presence of 100 μM $NADP^+$ and 2 mM Mn^{2+}. Shown are mean values of duplicate assays ±SD. The inset is an expanded view showing the IDH1 activities at lower isocitrate concentrations. (**D**) Cellular α-KG levels decrease with increasing IDH1^{R132H} expression. The upper panel is a Western blot showing expression levels of the transfected IDH1^{R132H} mutant in U-87MG cells. The α-KG level in cells transfected with empty vector was set as 100%, and this value was used to calculate the relative α-KG level in cells transfected with different amounts of IDH1^{R132H} mutant. Shown are mean values of triplicate assays ±SD.

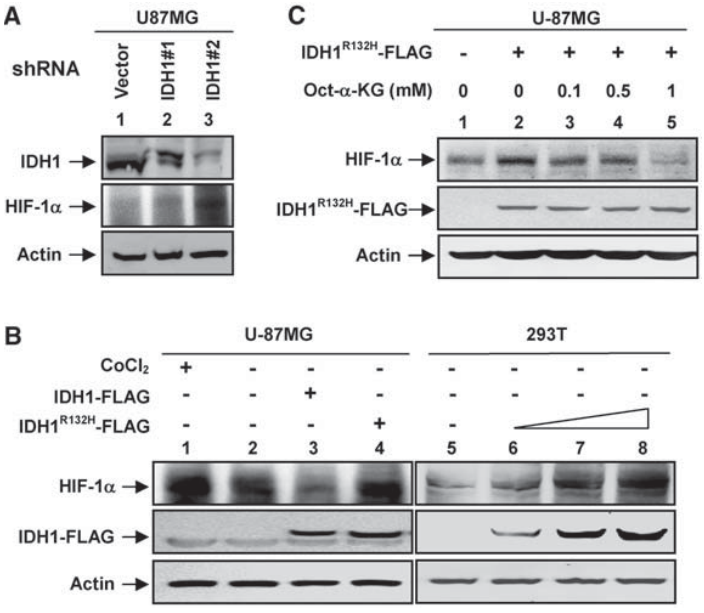

Fig. 3. α-KG mediates the HIF-1α induction in cells with a decreased IDH1 activity. (**A**) *IDH1* knockdown elevates HIF-1α levels in U-87MG glioblastoma cells. IDH1 and HIF-1α protein levels were determined by Western blotting from stable U-87MG cells transduced with empty retrovirus or retrovirus expressing different shRNAs silencing *IDH1*. (**B**) Ectopic expression of the *IDH1*^{R132H} mutant elevates HIF-1α levels in U-87MG and HEK293T cells. The *IDH1*^{R132H} mutant was overexpressed in U-87MG or HEK293T cells, and protein levels were detected by Western blot. $CoCl_2$-treated cells (a mimetic of hypoxia) and cells overexpressing wild-type *IDH1* were also included as controls. (**C**) A cell-permeable α-KG derivative blocks HIF-1α induction in cells expressing *IDH1*^{R132H}. The U-87MG cells were transfected with *IDH1*^{R132H}, and different concentrations of octyl-α-KG ester were added to each transfected cell for 4 hours. HIF-1α protein levels were assayed by Western blot.

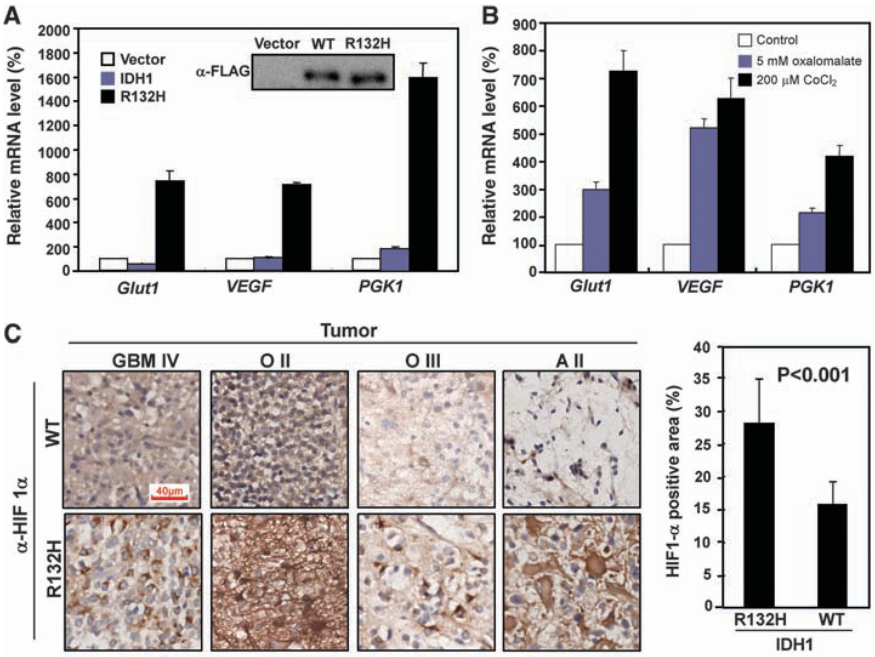

Fig. 4. IDH1 activity affects the levels of HIF-1α and HIF-1α target genes in gliomas and cultured cells. (**A**) Overexpression of the *IDH1*^{R132H} mutant in U-87MG cells stimulates expression of HIF-1α target genes (*Glut1, VEGF*, and *PGK1*) as assayed by QPCR. Shown are mean values of triplicate assays ±SD. (**B**) Inhibition of IDH1 by oxalomalate activates HIF-1α target genes. U-87MG cells were either untreated (control), treated with 5 mM oxalomalate, an IDH1 inhibitor, or treated with $CoCl_2$, a hypoxia mimetic. HIF-1α target gene mRNAs were determined. Shown are mean values of triplicate assays ±SD. (**C**) Immunohistochemistry of HIF-1α was carried out in 12 human gliomas with wild-type *IDH1* and 8 gliomas of similar grade harboring a mutated *IDH1* allele. Shown are side-by-side comparisons of four gliomas representing different types or grades. Scale bar, 40 μM. Five fields (~173 μm^2 each) were randomly selected from each sample for quantification of HIF-1α-positive staining area. Statistical analysis was performed using seven *IDH1* wild-type and seven *IDH1*-mutated gliomas.

factor 1α (HIF-1α), we hypothesized that decreased IDH1 activity might stabilize HIF-1α and increase its steady-state levels. We found that HIF-1α protein levels in U-87MG cells were elevated in response to shRNA-mediated knockdown of *IDH1* (Fig. 3A). Conversely, overexpression of wild-type IDH1 reduced HIF-1α protein levels in HeLa (fig. S5A) and U-87MG cells (Fig. 3B). Notably, overexpression of *IDH1*^{R132H} mutant increased HIF-1α protein levels in U-87MG and HEK293T cells (Fig. 3B). These results suggest that IDH1 regulates HIF-1α levels by controlling the level of α-KG. We tested this hypothesis by treating cells with octyl-α-KG, a cell-permeable derivative of α-KG that upon entering the cells is converted into α-KG after hydrolysis of the ester group (*10*). We found that octyl-α-KG suppressed the HIF-1α induction caused by either *IDH1* knockdown in HeLa cells (fig. S5B) or overexpression of *IDH1*^{R132H} mutant in U-87MG cells (Fig. 3C). We therefore conclude that a reduction in IDH1 activity produces a reduction in α-KG levels that in turn can lead to stabilization of HIF-1α.

We next determined whether inhibition of IDH1 enzyme activity leads to up-regulated expression of HIF-1α target genes. HIF-1α is a key component of HIF-1, a transcription factor that senses low cellular oxygen levels and that regulates the expression of genes implicated in glucose metabolism, angiogenesis, and other signaling pathways that are critical to tumor growth. Quantitative real-time fluorescence polymerase chain reaction (QPCR) of mRNAs corresponding to three well-established HIF-1α target genes, glucose transporter 1 (*Glut1*), vascular endothelial growth factor (*VEGF*), and phosphoglycerate kinase (*PGK1*) showed that *IDH1* knockdown induced the expression of these HIF-1α target genes (fig. S6A). Moreover, expression of the *IDH1*^{R132H} mutant, but not wild-type *IDH1*, strongly induced HIF-1α target gene expression (Fig. 4A). Oxalomalate, a competitive inhibitor of IDH1 (*11*) (fig. S6B), also induced expression of these HIF-1α target genes (Fig. 4B).

Finally, we determined whether *IDH1* mutations correlate with elevated levels of HIF-1α in human gliomas. In a collection of 26 glioma samples, we identified 8 tumors that contained the R132H mutation in one allele of *IDH1* (table S1) (fig. S7A). Using immunohistochemistry, we compared HIF-1α expression in gliomas with and without *IDH1* mutations. We found that 8 tumors harboring the R132H mutation showed a statistically stronger HIF-1α signal than did 12 tumors that did not harbor this mutation (Fig. 4C). In *IDH1* mutated tumors, 28.1 ± 6.7% of the cells stained positive for HIF-1α, whereas in tumors with wild-type *IDH1*, only 15.8 ± 3.5% of the cells stained positive ($P < 0.001$) (Fig. 4C). *IDH1*-mutated gliomas also exhibited an increase in VEGF levels compared with gliomas without *IDH1* mutation of similar type and grade (fig. S7B).

In summary, we have shown that *IDH1* is likely to function as a tumor suppressor gene rather than as an oncogene. The glioma-associated mutations dominantly inhibit the activity of wild-type IDH1 through heterodimer formation (fig. S8). *IDH1* gene mutations in gliomas exhibit two unique features: the lack of LOH and the lack of apparent inactivating mutations such as frameshift or truncations. Our findings help to explain both features, as dominant inhibition would eliminate the selection pressure to mutate or lose the remaining wild-type allele (LOH) and frameshift or premature termination would likely generate IDH1 fragments unable to dimerize with and inhibit the wild-type IDH1 protein.

The link between *IDH1* and HIF-1α highlights an emerging theme in which mutationally altered metabolic enzymes are thought to contribute to tumor growth by stimulating the HIF-1α pathway and tumor angiogenesis. The genes encoding two TCA enzymes, fumarate hydratase (*FH*) and succinate dehydrogenase (*SDH*), have been found to sustain loss-of-function mutations in certain human tumors, which likewise correlate with an increase in HIF-1α levels (*10*, *11*). In addition to affecting PHD, an alteration in α-KG might contribute to tumorigenesis by affecting other dioxygenases that use α-KG as a substrate. IDH1 also catalyzes the production of NADPH; thus, it is possible that a reduction in NADPH levels resulting from IDH1 mutation contributes to tumorigenesis through effects on cell metabolism and growth. Several dozen anticancer agents directly targeting HIF-1α are under development or being tested (*12*). Our finding that an α-KG derivative can reverse the induction of HIF-1α levels in cultured cells expressing mutant *IDH1* suggests that drugs mimicking α-KG may merit exploration as a therapy for gliomas that harbor an *IDH1* mutation.

References and Notes

1. F. B. Furnari *et al.*, *Genes Dev.* **21**, 2683 (2007).
2. D. W. Parsons *et al.*, *Science* **321**, 1807 (2008).
3. J. Balss *et al.*, *Acta Neuropathol.* **116**, 597 (2008).
4. F. E. Bleeker *et al.*, *Hum. Mutat.* **30**, 7 (2009).
5. H. Yan *et al.*, *N. Engl. J. Med.* **360**, 765 (2009).
6. B. S. Winkler, N. DeSantis, F. Solomon, *Exp. Eye Res.* **43**, 829 (1986).
7. X. Xu *et al.*, *J. Biol. Chem.* **279**, 33946 (2004).
8. S. Soundar, B. L. Danek, R. F. Colman, *J. Biol. Chem.* **275**, 5606 (2000).
9. K. R. Albe, M. H. Butler, B. E. Wright, *J. Theor. Biol.* **143**, 163 (1990).
10. E. D. MacKenzie *et al.*, *Mol. Cell. Biol.* **27**, 3282 (2007).
11. O. C. Ingebretsen, *Biochim. Biophys. Acta* **452**, 302 (1976).

12. G. L. Semenza, *Drug Discov. Today* **12**, 853 (2007).
13. We thank members of the Fudan Molecular and Cell Biology Laboratory for valuable input; Y. Liu, X. Liu, and H. Zhu for assistance with histology; Z. Bao, L. Yang, Q. Shi, and G. Zhao for clinical samples; and S. Jackson for reading the manuscript. This work is supported by the 985 program from the Chinese Ministry of Education, State Key Development Programs of China (2009CB918401, 2006CB806700), National 863 Program of China (2006AA02A308), China NSF grants (30600112 and 30871255) and Shanghai Key Basic Research Projects (06JC14086, 07PJ14011, and 08JC1400900), and NIH grants (to K.-L.G. and Y.X.). Y. Xiong, K.-L. Guan, and S. Zhao are applying for a patent related to the work on permeable alpha-ketogluterate.

Supporting Online Material
www.sciencemag.org/cgi/content/full/324/5924/261/DC1
Materials and Methods
Figs. S1 to S8
Table S1

15 January 2009; accepted 10 March 2009
10.1126/science.1170944

Demonstration of Genetic Exchange During Cyclical Development of *Leishmania* in the Sand Fly Vector

Natalia S. Akopyants,[1]* Nicola Kimblin,[2]* Nagila Secundino,[2] Rachel Patrick,[2] Nathan Peters,[2] Phillip Lawyer,[2] Deborah E. Dobson,[1] Stephen M. Beverley,[1]† David L. Sacks[2]†‡

Genetic exchange has not been shown to be a mechanism underlying the extensive diversity of *Leishmania* parasites. We report here evidence that the invertebrate stages of *Leishmania* are capable of having a sexual cycle consistent with a meiotic process like that described for African trypanosomes. Hybrid progeny were generated that bore full genomic complements from both parents, but kinetoplast DNA maxicircles from one parent. Mating occurred only in the sand fly vector, and hybrids were transmitted to the mammalian host by sand fly bite. Genetic exchange likely contributes to phenotypic diversity in natural populations, and analysis of hybrid progeny will be useful for positional cloning of the genes controlling traits such as virulence, tissue tropism, and drug resistance.

Parasitic protozoa of the genus *Leishmania* cause a spectrum of human diseases that pose serious public health challenges for prevention, diagnosis, and treatment. The diversity of *Leishmania* species, with more than 20 currently recognized, is thought to have arisen by gradual accumulation of divergent mutations rather than by sexual recombination. Tibayrenc *et al.* (*1*) have reported strong linkage disequilibrium in several *Leishmania* species and proposed that these parasites are essentially clonal. This notion must be reconciled, however, with the accumulating examples of naturally occurring strains that share genotypic markers from two recognized species and thereby provide circumstantial evidence for sexual recombination (*2*–*4*). Genetic exchange has been documented for the other trypanosomatids that cause human disease. Hybrid genotypes were observed in tsetse flies during cotransmission of two strains of *Trypanosoma brucei* (*5*) and in mammalian cells after coinfection with two clones of *Trypanosoma cruzi* differing in drug-resistance markers (*6*). Using drug resistance markers, we provide evidence for genetic exchange in *Leishmania major* and discuss the implications of these findings to *Leishmania* biology and experimental analysis.

[1]Department of Molecular Microbiology, Washington University School of Medicine, St. Louis, MO 63110, USA. [2]Laboratory of Parasitic Diseases, National Institute of Allergy and Infectious Diseases, NIH, Bethesda, MD 20892, USA.

*†These authors contributed equally to this work.
‡To whom correspondence should be addressed. E-mail: dsacks@nih.gov

One parental clone, LV39c5(HYG), was derived from strain LV39 clone 5 (MHOM/SU/59/P) and was heterozygous for an allelic replacement of the *LPG5A* on chromosome 24 by a hygromycin B–resistance cassette (*LPG5A*/*LPG5A*::Δ*HYG*) (*7*). The second parental clone, FV1(SAT), was derived from NIH Friedlin clone V1 (MHOM/IL/80/FN) and bore a heterozygous nourseothricin–resistance (*SAT*) marker, integrated along with a linked firefly luciferase (*LUC*) reporter gene into one allele of the ~24 rRNA cistrons located on chromosome 27 (*8*) (+/*SSU*::*SAT-LUC*). These strains were chosen as they are phenotypically identical to their respective parental wild-type (WT) virulent *L. major*; whereas the markers were chosen because they are functionally independent (*9*). The target gene modifications were chosen because they caused no effect on normal growth in vitro or in mouse infections (*10*), and epistatic interactions were not anticipated between these alleles.

Multiple attempts to generate hybrid parasites resistant to both antibiotics during *in vitro* coculture of the parental lines were unsuccessful (*11*). The parental clones were tested for their ability to generate parasites resistant to both drugs during coinfection in the sand fly. The growth of each parental line in *Phlebotomus duboscqi,* a natural vector of *L. major*, is shown in fig. S1. Promastigotes of each parent survived the initial period of blood-meal digestion and excretion (days 1 to 6) and underwent metacyclogenesis at a comparable frequency (20 to 60%), although the FV1(SAT) parent established and maintained a higher intensity of infection by a factor of 3 to 4. The parental clones were tested for their ability to generate doubly drug–resistant parasites during coinfection in the sand fly. Flies were fed through a membrane on mouse blood containing 3 and 1×10^6/ml of the LV39c5(HYG) and FV1(SAT) lines, respectively, each obtained from log-phase cultures and extensively washed to remove antibiotics. A total of 102 flies from four independent coinfection experiments were dissected 13 to 16 days postinfection; at this time, they harbored mature infections with an average of 39,400 ± 14,700 promastigotes per midgut. Flies cannot be maintained under aseptic conditions, and more than half of the cultures established from the midgut parasites were lost to fungal contamination during the subsequent 1 to 2 weeks of culture. In the remaining cultures, 12 (26%) grew out promastigotes that were resistant to both drugs. Clonal lines were generated from nine of the doubly drug–resistant populations, and the genotypes and phenotypes of one or two clones from each culture were determined (summarized in Table 1).

Polymerase chain reaction (PCR) tests with primers specific for the parental markers showed that all doubly drug–resistant clones tested contained both the *HYG* and *SAT* drug-resistance genes (Fig. 1A, Table 1, and table S3). Controls showed that the marker loci had not rearranged during hybrid formation but had maintained their location within the *LPG5A* or *SSU* rRNA loci, respectively (fig. S2). These data indicated that the doubly drug–resistant clonal lines were genetic hybrids. To confirm that hybrid formation was compatible with transmission to the mammalian host, coinfected sand flies were allowed to bite and to induce lesions in BALB/c mice. Two doubly drug–resistant clonal lines, designated 6.16.E8 and 6.14.F9, were recovered from the eight dermal lesions examined and were found to be similar to those directly recovered from insects, as discussed below (Table 1). Coinjection of both parental lines into mouse ears by needle never led to the recovery of doubly drug–resistant parasites from the 20 dermal lesions examined, each containing $>2.4 \times 10^7$ amastigotes, which suggested that the hybrids selected after transmission by the coinfected sand flies were generated in the fly and not in the mammalian host.

We examined the segregation of loci not linked to chromosomes 24 and 27, the location of the *HYG* and *SAT* markers, respectively. We used single-nucleotide polymorphisms (SNPs) developed from comparisons of the terminal ~30-kb chromosomal regions encompassing the *SCG* genes located on *L. major* chromosomes 2,